Updated systematics of intermediate-energy single-nucleon removal cross sections

J. A. Tostevin [1] and A. Gade [2,3]

[1]*Department of Physics, Faculty of Engineering and Physical Sciences, University of Surrey, Guildford, Surrey GU2 7XH, United Kingdom*
[2]*National Superconducting Cyclotron Laboratory, Michigan State University, East Lansing, Michigan 48824, USA*
[3]*Department of Physics and Astronomy, Michigan State University, East Lansing, Michigan 48824, USA*

(Received 16 January 2021; accepted 10 May 2021; published 19 May 2021)

The body of experimental measurements of intermediate-energy reactions that remove a single nucleon from a secondary beam of neutron- or proton-rich nuclei continues to grow. These data have been analyzed consistently using an approximate, eikonal-model treatment of the reaction dynamics combined with appropriate shell-model descriptions of the projectile initial state, the bound final states spectrum of the reaction residue, and single-particle removal strengths computed from their wave-function overlaps. The systematics of the ratio R_s of the measured inclusive cross section to all bound final states and the calculated cross section to bound shell-model states—in different regions of the nuclear chart and involving both very weakly bound and strongly bound valence nucleons—is important in relating the empirically deduced orbital occupancies to those from the best available shell-model predictions. Importantly, several new higher-energy measurements, for which the sudden-approximation aspect of the dynamical description is placed on an even stronger footing, now supplement the previously analyzed measurements. These additional data sets are discussed. Their R_s values are shown to conform to and reinforce the earlier-observed systematics, with no indication that the approximately linear reduction in R_s with increasing nucleon separation energy is a consequence of a breakdown of the sudden approximation.

DOI: 10.1103/PhysRevC.103.054610

I. INTRODUCTION

Measurements and eikonal-model analyses of single-nucleon removal reactions from rare-isotope beams at intermediate energy (energies in excess of 80 MeV/nucleon) have been invaluable in advancing our understanding of single-particle degrees of freedom and the evolution of shell structure with increasing neutron-proton number asymmetry [1]. This, in turn, has helped advance the development of new shell-model effective interactions; see, for example, Refs. [2–5]. A global feature of this increasing body of precision removal-reaction data is the behavior of the ratio, denoted R_s, of the measured and eikonal-model absolute inclusive cross sections to all bound final states of the residual nucleus. This behavior is seen in the totality of data from very different regions of the nuclear chart and including nuclei with extreme $A:Z$ number ratios. These involve nucleon removals from both very weakly bound and well-bound valence single-particle orbitals near their respective Fermi surfaces. These deduced ratios, as a function of the separation energy asymmetry ΔS of the two nucleon species, defined below, show a characteristic and essentially linear behavior; decreasing from values near unity for removals of the most weakly bound nucleons to values $\approx 0.3(1)$ for the most strongly bound nucleon cases.

A first compilation, noting this behavior and detailing the model calculations, was presented in Ref. [6]. That work included three data points with energies between 60 and 70 MeV/nucleon and also incorporated the earlier analysis [7] of high-energy data for the $^{12}\mathrm{C}(-n,-p)$ and $^{16}\mathrm{O}(-n,-p)$ reactions, at 250, 1050, and 2100 MeV/nucleon. The latter showed consistency with the analogous cross-section ratios deduced from high-energy electron-induced proton knockout from these and other stable nuclei. This initial data compilation was subsequently enhanced in Ref. [8], with the addition of new data analyses, the majority of which were from measurements in the 80–120 MeV/nucleon range. Here, we add additional information to these growing systematics. Importantly, we include several additional data points derived from new measurements at significantly higher energies. These now include reactions at the positive and negative extremes of ΔS.

II. REACTION MODEL

The eikonal-model theoretical description of the nucleon removal reaction dynamics used in the analyses of these collisions—of a projectile of mass A with a light target nucleus—uses the sudden (fast collision) and eikonal (forward scattering) approximations. These ingredients have been presented and discussed in detail elsewhere; see, for example, Refs. [9,10] and the references therein. The key dynamical ingredients that enter the model cross-section calculations are the elastic S matrices of the removed nucleon and the mass $A-1$ reaction residue, expressed as a function of their collision impact parameters. These S matrices describe the degree of transmission and absorption of these particles as

they transit the complex (optical-model) interactions with the target nucleus. These highly absorptive optical interactions, in particular that of the ion-ion (residue-target) system, dictate that the single-nucleon removing events, which require the transmission (survival) of the mass $A-1$ residues, are entirely dominated by impact parameters that involve only grazing contact of the nuclear surfaces and that do not penetrate into the nuclear interior. Such interior collisions, at smaller impact parameters, result in more complex fragmentation channels with essentially complete absorption of the mass $A-1$ residues. As a result of this surface dominance of the single-nucleon removal mechanisms, the strong-interaction path lengths along which the nucleon and residual nucleus transit their optical potentials with the light-target nucleus are of short range and the interaction time is correspondingly short.

A. Sudden approximation

This strongly absorptive potential behavior, the geometry of the optical potentials, and the surface dominance of the removal reaction events are largely unchanged in the calculations for all incident energies of interest, i.e., those in excess of 80 MeV/nucleon. So, the collision or transit time is essentially dictated by the energy (velocity) of the projectile beam. For example, at 100 MeV/nucleon, with $\gamma = 1.1$, $v/c \approx 0.4$ and the estimated collision time $\mathcal{T}_{\rm coll}$ is of order $8 \times d \times 10^{-24}$ s, where d (in fm) is the typical strong-interaction path length. Given the light target nuclei used, with root mean squared (rms) matter radii of 2.36 fm (Be) and 2.32 fm (C), these expected path lengths are of order 2–4 fm. Such collision times are faster than conventional light-ion direct-reaction times and those typically associated with any significant motion of valence nucleons near the nuclear surface (and the Fermi surface) in the nuclear ground state. These timescales are the basis of the sudden (sometimes referred to as the fast-adiabatic) approximation: that the vector separation between the removed nucleon and the residual nucleons in the projectile ground state can be treated as frozen for the short duration of the collision, $\mathcal{T}_{\rm coll}$.

The magnitude of the leading-order correction to this sudden (fast-adiabatic) approximation in the case of the simpler elastic breakup mechanism was considered in some detail by Johnson [11] and Summers *et al.* [12] for weakly bound projectiles. The elastic breakup mechanism is an important, although not the dominant, removal mechanism in well-bound nucleon removal cases, as is quantified below. Importantly, however, these studies also concluded, as was argued above, that the spatial localization of this removal reaction mechanism arising from the strongly absorptive residue-target interaction, removes the major part of the nonadiabatic corrections—the maximum of the leading correction term lying at smaller impact parameters at which the strong absorption has reduced the S matrix is essentially zero. Such a formal analysis is very difficult in the case of the inelastic breakup mechanism where the presence of a continuum of target excitations to unbound configurations destroys the simpler, three-body-like nature of the elastic breakup dynamics. Hence, we confine discussion to the short collision time that underpins the sudden approximation, dictated by the energy of the projectiles.

Clearly, this collision time $\mathcal{T}_{\rm coll}$ becomes shorter as the beam energy is raised. This reduction is by a factor of $\approx 2/3$ when the beam energy exceeds 240 MeV/nucleon, For more highly relativistic, 1.6 GeV/nucleon projectiles, the energy of several new precision measurements at which $v/c \approx 0.92$, $\mathcal{T}_{\rm coll}$ is reduced by more than a factor of 2. So, a comparison of the cross sections and R_s deduced from the existing data (most at $\approx$ 100 MeV/nucleon) and higher-energy measurements over such an extended energy range may be expected to reveal differences if there is any significant breakdown of the accuracy of the sudden approximation in the analyses of the lower-energy data points. This comparison motivates the present study.

B. Other reaction considerations

The intermediate energy of the projectile beam is essential for the sudden and eikonal dynamical approximations to be applicable. A minimum beam energy is also of particular importance for the points with large positive ΔS, the cases where the removed nucleons are most strongly bound. The kinematics in these large negative Q-value reaction cases naturally imposes an upper limit upon the longitudinal momentum carried by the fast, forward-traveling reaction residues. This was shown dramatically in Ref. [13], where the ^{14}O$(-n)$ reaction, with $S_n = 23.2$ MeV, was performed at too low a secondary beam energy of 53 MeV/nucleon. There, this kinematical cutoff was sufficiently low that it intruded into and distorted the conventionally Gaussian-like longitudinal momentum distribution of the ^{13}O residues. An expression for this maximal beam-direction residue momentum was given in Ref. [8]. That analysis, like that of Ref. [13], concluded that, even for the maximum nucleon separation energies expected physically, this kinematic cutoff has minimal effect for reactions with beam energies close to and in excess of 80 MeV/nucleon. So, this kinematics-cutoff effect has no implications for the higher-energy data sets we discuss here.

The additional dynamical approximation made in the model calculations is that the mass $A-1$ reaction residue is treated as a spectator and its internal state, α, is preserved in the collision. Use of the spectator approximation is critical to the spectroscopic usefulness of the reaction, since the yield of residues in a particular final state α then reflects the component (parentage) of this configuration in the ground-state wave function of the projectile. This assumption is not explicitly studied here and is assumed in all calculations, regardless of the separation energy of the removed nucleon. Nevertheless, since measured and calculated ion-ion inelastic cross sections fall with increasing collision energy, it is expected that the spectator approximation will also improve with the projectile energy.

It is important to remember that the measured and calculated removal cross sections are highly inclusive with respect to the (unobserved) final states of the target nucleus, being ^{9}Be and ^{12}C in all cases considered. For these low Z target nuclei, nucleon removal due elastic Coulomb dissociation can be neglected. Rather, the two strong-interaction driven

nucleon removal mechanisms, elastic and inelastic breakup of the projectile, are the dominant processes [10], in which the target nucleus remains in or is excited from its ground state. For reactions on these light target nuclei the inelastic breakup (or stripping) mechanism drives the larger part of the removal cross section, the fraction due to the elastic breakup mechanism being between 40% and 17% in the cases where the relative yields of these processes have been distinguished by measurements [14,15]. The fractions of these elastic and inelastic removal events predicted by the eikonal-model calculations, which depend strongly on the nucleon separation energy, are in excellent agreement with the results of these dedicated measurements for removals from both weakly bound [14] and well-bound [15] orbitals. Here we discuss only the sum of these two contributions that, in general, are not distinguished.

Until somewhat recently, measurements have routinely determined only the total number of bound, mass $A-1$ residues. The cross section measurements presented here are also inclusive with respect to all bound final states of the reaction residue. For many of the rare, highly neutron-proton-number asymmetric nuclei used, these bound final-states spectra are unknown or only partially known. The model analyses thus take the final-state spins, parities, and excitation energies from shell-model calculations with effective interactions and model spaces appropriate to the mass and charge of the projectile. The theoretical inclusive cross sections are taken as the sum of the calculated partial cross sections to all of the shell-model states of the residue with predicted excitation energies consistent with the empirical, if known, or the evaluated lowest particle emission threshold and its uncertainty; that is, S_n for neutron-rich or S_p for neutron-deficient residues.

III. ANALYSIS AND RESULTS

A. Methodology

We summarize the analysis methodology that is applied to each reaction. The theoretical partial cross section for removal of a nucleon, from a single-particle configuration j^π, populating the residue final state α with excitation energy E^*_α, is calculated as [10]

$$\sigma_{\rm th}(\alpha) = \left(\frac{A}{A-1}\right)^N C^2S(\alpha, j^\pi)\,\sigma_{\rm sp}\left(j, S^*_\alpha\right), \qquad (1)$$

where $S^*_\alpha = S_{n,p} + E^*_\alpha$ is the separation energy to the final state α and $S_{n,p}$ is the ground-state to ground-state nucleon separation energy. N, in the A-dependent center-of-mass correction to the shell-model spectroscopic factors, $C^2S(\alpha, j^\pi)$, is the number of oscillator quanta associated with the major shell of the removed particle [16]. The single-particle cross section $\sigma_{\rm sp}$ is the sum of the elastic and inelastic breakup contributions to the reaction [9] calculated assuming the removed nucleon's single-particle wave function (or overlap function) is normalized. The theoretical inclusive nucleon-removal cross section, $\sigma_{\rm th}$, is then the sum of these partial cross sections to all bound final states of the mass $A-1$ residue. This cross section is thus the predicted reaction yield resulting from the single-particle strengths to the low-energy spectrum of the residue. As should be clear from the above, this inclusive cross section does not probe the values of individual spectroscopic factors, $C^2S(\alpha, j^\pi)$. The overall shell-model strength to bound final states can, however, be compared with the measured cross sections, $\sigma_{\rm exp}$. This is the basis and physics of the cross sections ratio $R_s = \sigma_{\rm exp}/\sigma_{\rm th}$.

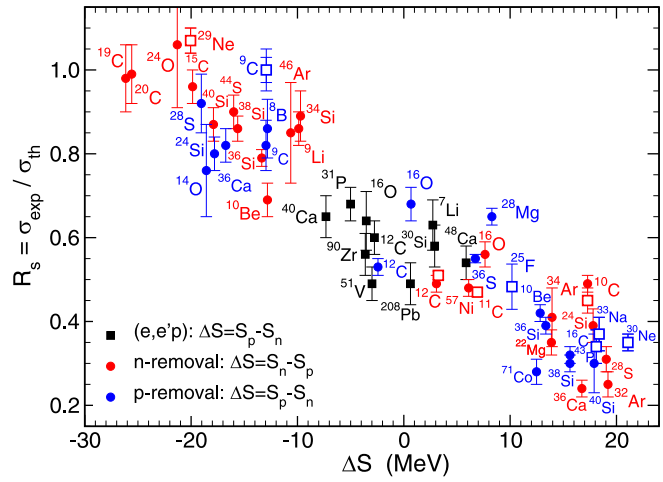

FIG. 1. Compilation of the computed ratios, R_s, of the experimental and theoretical inclusive one-nucleon removal cross sections for each of the projectile nuclei indicated. R_s is shown as a function of the parameter ΔS, used as a measure of the asymmetry of the neutron and proton Fermi surfaces. The new red (neutron removal) and blue (proton removal) higher-energy data points are shown as open squares. The solid (black) squares, deduced from electron-induced proton knockout data, are identical to those in the original compilation of Ref. [6].

The asymmetry of the neutron and proton separation energies from the orbitals near their Fermi surfaces is quantified, in each reaction, by the parameter ΔS. If only the residue ground state is bound then $\Delta S = S_n - S_p$ for neutron removal and $\Delta S = S_p - S_n$ for proton removal. When there are several bound shell-model final states the separation energy of the removed particle in ΔS, above, is replaced by the partial-cross-section weighted average of these bound states S^*_α. With this convention, the removal of the most strongly-bound (weakly bound) nucleons from proton-neutron asymmetric nuclei have large positive (negative) values of ΔS. The deduced R_s and ΔS for the body of data sets are shown in Fig. 1.

The inputs to the $\sigma_{\rm th}$ calculations: the ranges of the optical potentials and of the nucleon radial overlaps, which dictate the reaction geometry, must be chosen consistently [6]. Each $\sigma_{\rm th}$ calculation requires realistic: (i) final-states spectra and C^2S, (ii) residue- and nucleon-target optical potentials and their derived elastic S matrices, which localize the reactions spatially, and (iii) removed-nucleon radial wave-function geometries from the projectile ground state. For (i) we use the best available shell-model calculations and for (ii) and (iii) we constrain the shapes and radial size parameters using theoretical, Hartree-Fock (HF) model systematics. The errors on the calculated $\sigma_{\rm sp}$, arising from the precise values of these sizes (rms radii) of the nucleon radial wave functions and those of the residual and target nuclei, with which the cross sections scale essentially linearly [6], have been estimated

using finite-difference derivatives. These were summarized in Eq. (3) of Ref. [17] and Eq. (5) of Ref. [18] for removals from weakly bound and well-bound orbitals, respectively. The likely errors from this source, typically 10% (strongly bound cases) and 5% (weakly bound cases) for a δR uncertainty of 0.1 fm, are modest and confirm that the model calculations are robust against plausible changes to these theoretically constrained geometric inputs. The variation of the computed R_s when using different Skyrme forces in the HF calculations used to constrain these radial sizes were shown to be rather minimal; see for example Fig. 7 of Ref. [6]. All calculations presented here use the SkX Skyrme interaction [19]. More complete details of the procedures used, common to all of the data sets, are detailed in Refs. [6,8].

We add that, as most of the earlier data sets analyzed, and several of the new data sets included here, are for beam energies close to 100 MeV/nucleon on a ^{9}Be target, the removed nucleon-target nucleus optical potential and S matrix used in the analyses are essentially the same for the majority of the data sets across the full range of ΔS values. It follows that details of this optical potential can play little part in the observed behavior of R_s with ΔS.

B. Additional data sets

The data compilation in Fig. 1 includes all cases reported in Ref. [8]. These included a number of higher-energy measurements. For example, the ^{19,20}C$(-n)$ and ^{14}O$(-p)$ data points, with large negative ΔS, were made at 240 and 305 MeV/nucleon, respectively.

The updated figure includes the results of several new reported measurements in the 80–100 MeV/nucleon range. From left to right in the figure, these added analyses are for: ^{24}O$(-n)$ [20], ^{44}S$(-n)$ [21], ^{34}Si$(-n)$ [22], ^{36}S$(-p)$ [23], ^{71}Co$(-p)$ [24], and ^{43}P$(-p)$ [25]. Each of these new measurements was performed at the National Superconducting Cyclotron Laboratory's Coupled Cyclotron Facility, located at Michigan State University [26]. All of these additional systems are seen to be consistent with the established trend of the collected data.

Of particular interest are the additions, shown as open square symbols, from higher-energy measurements and model calculations at 220–240 MeV/nucleon and 1.6 GeV/nucleon. The 220–240 MeV/nucleon additions are, from left to right, for ^{29}Ne$(-n)$ [27], ^{25}F$(-p)$ [28], ^{16}C$(-p)$ [29], ^{30}Ne$(-p)$ [30], and ^{33}Na$(-p)$ [31]. For the ^{25}F$(-p)$ measurement, made on a carbon target at 218 MeV/nucleon, the data point is computed using the inclusive cross section reported informally in Ref. [28]. The shell-model calculation in that case used the universal sd-shell USDB effective interaction [32], the only significant transition being $d_{5/2}$ proton removal populating the ^{24}O ground state with a spectroscopic factor of 1.01 [33]. This gives an R_s value of 0.48(5) with $\Delta S = 10.17$ MeV.

All measurements, except that for ^{16}C$(-p)$, were performed at the Radioactive Isotope Beam Factory (RIBF) at RIKEN, Japan. The ^{16}C measurement was made at the External Target Facility, Institute of Modern Physics, Lanzhou, China. All data sets have been reanalyzed with the earlier-stated methodology, so the deduced R_s may differ in detail

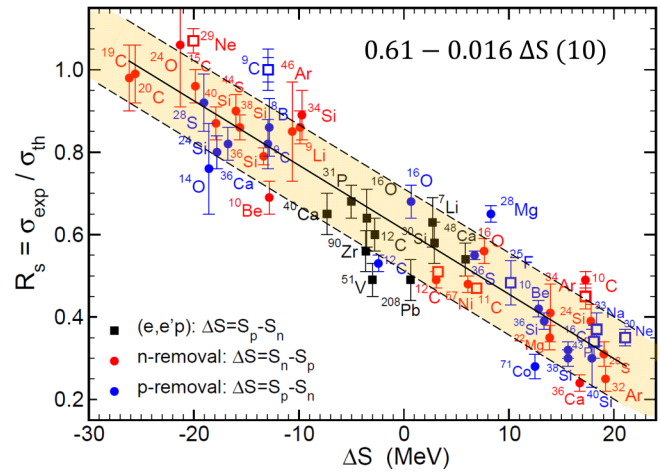

FIG. 2. As for Fig. 1. The trend line given in Eq. (2), as reported in Ref. [23], and a band of half-width 0.1 (shaded region) have been superimposed, which summarize the totality of collected data points.

where published values used different inputs. Specifically, the ^{16}C$(-p)$ data point in Fig. 1, deduced from the cross section reported in Ref. [29], is $R_s = 0.34(4)$ with a ΔS value of 18.1 MeV.

The added data points at 1.6 GeV/nucleon are for the carbon isotopes: ^{9}C$(-p)$, ^{12}C$(-n)$, ^{11}C$(-n)$, and ^{10}C$(-n)$, measured at the GSI Helmholtzzentrum für Schwerionenforschung, Darmstadt, Germany. The analyses of these measurements are detailed in Ref. [34]. For the new ^{9}C$(-p)$ and ^{10}C$(-n)$ reaction data, where there were also earlier, lower-energy analyses [35] at 100 and 120 MeV/nucleon, respectively, the agreement of the deduced R_s at the two energies is excellent.

Each of these independent data analyses, for projectiles across the nuclear chart and spanning the full extent of nucleon separation energies (and ΔS), are found to fall within the band of scatter of values of the earlier published systematics [8]. We note that, as was stated in Ref. [23], and as presented graphically in Fig. 2, a linear representation of the entire collection of data in Fig. 1 is provided by the trend line

$$R_s = 0.61 - 0.016\,\Delta S \qquad (2)$$

together with a scatter in the deduced R_s values, from the different regions of the nuclear chart, of order 0.1, independent of the ΔS value. This scatter of deduced values is not surprising given the very diverse set of projectile nuclei involved and the distinct shell-model spaces and effective interactions involved in the analyses of each of the different mass and charge regions.

It is important to stress that the presented R_s systematics provide an overall, sum-rule-like, inclusive measure of the theoretically predicted strength of transitions to bound final states, and do not provide information on any individual transition or spectroscopic factor. In particular, R_s is not an overall scaling factor to be applied to each contributing theoretical partial cross section. The relationship between the model and measured partial cross sections is expected to be far more complex. For example, in the recent ^{34}Si$(-n)$

reaction analysis included above [22], the measured and model partial cross sections to $3/2^+$ and $1/2^+$ ^{33}Si final states are in broad agreement. On the other hand, the model calculations predicted a number of strongly populated $5/2^+$ final states, that enhance the theoretical inclusive cross section, whereas these $5/2^+$ states were found to be more weakly populated in the measurements. So, to better interpret the deduced R_s value in each case requires more final-states-exclusive studies, as are now possible more routinely given the ongoing improvements in both beam intensities and detection capabilities.

C. Discussion

For the majority of spectroscopic applications, the details of these absolute cross section comparisons, as quantified by R_s, are secondary. As in essentially all direct-reaction applications, principally, it is comparisons of the measured and theoretical relative partial cross sections to each final state and, in intermediate-energy removal reactions, the shapes of their residue momentum distributions, that allow both the dominant transitions and single-particle configurations of the valence nucleons in the projectile ground state to be identified. The absolute inclusive cross-section comparisons, shown in Figs. 1 and 2, pose additional and challenging questions of both the reaction dynamics treatment and the nuclear structure model inputs. The following discussion summarizes aspects of ongoing investigations relevant to these open questions.

The physical origins of the presented systematic behavior, with a reduction of R_s with increasing ΔS, obtained consistently from the eikonal- plus sudden-approximation reaction dynamics and shell-model nuclear structure, remain unresolved. Testing for inadequacies in the reaction dynamics treatment, e.g., of the sudden approximation, was a motivation of the present work, using higher-energy data sets. Concerns regarding the shell-model nuclear-structure input, in particular the role and treatment of correlations in the many-body wave functions, are also relevant. The localization of the reaction, discussed earlier, means that absolute cross sections are particularly sensitive to the wave functions (overlap functions) of the removed nucleons near the nuclear surface, where the importance of neutron-proton correlations is an open question. Specifically, in reactions with large positive ΔS and at radii near the nuclear surface, the removed, minority nucleon species occupying orbitals near their energetically well-bound Fermi surface are embedded, spatially, within nuclear matter that is dominated by the other, majority species. We return to this discussion below.

Given these open questions, other nucleon-removal mechanisms, direct-reaction models and experimental data have also begun to be used to probe these absolute cross-section effects. Reference [36] presents a comprehensive recent review of these studies, which, to date, involve a more limited set of projectile species than used here. These alternative reactions involve different spatial localizations and radial sensitivities, and bring their own approximation schemes, model inputs, and uncertainties. For example, measured and theoretical cross-section ratios have been presented using analyses of single-nucleon transfer reactions [37–39], analyzed using conventional distorted-waves Born-approximation-like techniques, and inverse kinematics $(p, 2p)$ and (p, pn) knockout processes on a proton target, analyzed using quasifree scattering [40,41] and coupled-channels approaches [42]. In the case of the transfer reaction analyses, experimental (beam-intensity and target-thickness) requirements have limited the range of ΔS values accessible, while the ratios presented are generally from selected exclusive (e.g., ground-state) cross sections and not from the bound final state inclusive yields. The $(p, 2p)$ and (p, pn) knockout analyses cover a wider range of ΔS values but have been concentrated on the oxygen and carbon isotopes, with very few cases in common with the compilation in Fig. 1. An exception is an inverse kinematics $(p, 2p)$ measurement of the ^{25}F$(-p)$ reaction [33], which deduced an empirical spectroscopic factor of 0.36(13) to the ^{24}O ground state, the only bound final state. The corresponding new measurement on a C target was included above. Compared to shell-model values, the spectroscopic factor from this $(p, 2p)$ measurement is more heavily suppressed than the value from the higher-precision C target data, from which the deduced empirical spectroscopic factor, $\sigma_{\rm exp}/\sigma_{\rm sp}$, is 0.53(6). A program of precision measurements, on a common set of projectile and residue nuclei, using these alternative removal mechanisms, with their different spatial sensitivities to the wave functions of the removed nucleons, would be of considerable value in making direct comparisons.

Overall, and based on their more-limited reaction data sets, the ratios of the measured and reaction model cross sections from the transfer, $(p, 2p)$ and (p, pn) reaction analyses are more constant as a function of ΔS than is shown in Figs. 1 and 2. In contrast, a recent and completely different reaction methodology, the intra-nuclear-cascade (INC) model [43], applied to inclusive cross sections from fast neutron- and proton-removal reactions from medium-mass neutron-rich nuclei on a beryllium target at energies near 1 GeV/nucleon, deduced highly asymmetric $\sigma_{\rm exp}/\sigma_{\rm th}$ ratios between the neutron- and proton-removal channels. There, as in the present work, the calculated cross sections for the well-bound, large positive ΔS proton-removal cases significantly exceeded the measured values. The conclusion drawn from that study was that the absence of a realistic treatment of short-range correlations in the INC-model calculations was principally responsible for this outcome. As that more-macroscopic model approach also uses only very limited nuclear structure input, and not the detailed shell-model final states and spectroscopic information used in the model of this work, the ratios of cross sections deduced in Ref. [43] are not the same as the R_s defined here.

Regarding these shell-model theoretical inputs, it is reasonable to expect that the actual physical spectroscopic strengths will be somewhat suppressed compared to those computed in the highly truncated model spaces of practical shell-model calculations. This effect has not yet been fully quantified. Relevant, however, are the extensive recent nucleon-nucleon (NN) short-range correlation (SRC) studies probed using high-energy electron beams, e.g., [44–46]. These data show conclusively that, for higher nucleon momenta, SRC effects are dominated by neutron-proton pairs and that, in nuclei with a neutron excess, the minority proton species have a

significantly greater probability to be found with momenta above their Fermi momentum than do the neutrons [47]. This was interpreted as due to the action of the NN tensor force. A phenomenological approach to see the effect of these correlations on calculated electron- and proton-induced knockout cross sections from stable and asymmetric nuclei was presented in Ref. [48]. A conclusion was that the increased proton high-momentum components may, under certain assumptions, result in reduced occupancies and spectroscopic factors for proton orbitals near their Fermi surface. Our expectation is that the action of these neutron-proton SRCs, between the minority valence protons and the excess of neutrons, that occupy less-well-bound but spatially overlapping orbitals, will elevate some fraction of the valence protons to otherwise empty orbitals above their Fermi surface. Such excited, normally unoccupied proton orbitals are not conventionally included in the spaces of shell-model calculations, as used in this work. The shell-model occupancies of the valence nucleons, confined to orbitals in the restricted model space, are thus expected to be somewhat enhanced. This effect needs further and quantitative investigation.

The major part of these alternative efforts, and the present analysis, have concentrated on the reduced R_s values at large positive ΔS, those most likely to be impacted by any failings of the sudden approximation to the dynamics. There remains very limited discussion of the deduced larger R_s in systems with large negative ΔS – the removal of very weakly bound and halolike nucleons. These R_s, with values near unity, are an equally strong feature of the data and model systematics and, based on the discussions above, signal that the correlations experienced by these spatially extended valence nucleons, beyond those included approximately through the shell-model effective interactions, may be significantly reduced. However, since there is no explicit treatment of the continuum in the shell-model calculations used here, these questions cannot be addressed quantitatively within the presented model. We have shown, however, that these systematics are a robust feature of the eikonal plus shell-model analyses and that these are reinforced by the additional, newly available measurements, that include data at significantly higher beam energies.

IV. CONCLUSION

We have reported comparisons of measured and calculated inclusive single nucleon removal cross sections for additional reactions, including many at significantly higher beam energies. For these higher-energy data, the collision time is correspondingly shorter and the validity of the sudden approximation in the collision dynamics is thus enhanced. Analyses of these new measurements, that include energies from around 100 MeV/nucleon up to 1.6 GeV/nucleon, agree with the earlier-noted trends of the ratio of the measured and theoretical cross sections, $R_s = \sigma_{\rm exp}/\sigma_{\rm th}$, with the neutron-proton separation energy asymmetry parameter ΔS. The results from these new data sets, which span the full range of ΔS values, show no significant deviations from the earlier data analyses or indicate any breakdown of the sudden approximation in the analyses of these and the numerous other measurements in the energy range of 80–120 MeV/nucleon.

ACKNOWLEDGMENTS

The authors thank Prof. Joachim Enders (TU Darmstadt) and Prof. Takashi Nakamura (Tokyo Institute of Technology) for information on and citations to their Groups' recently-analysed data sets. This work was supported by the United Kingdom Science and Technology Facilities Council (STFC) under Grant No. ST/F005314/1 and by the U.S. Department of Energy, Office of Science, Office of Nuclear Physics, under Grant No. DE-SC0020451.

[1] A. Gade and T. Glasmacher, Prog. Part. Nucl. Phys. **60**, 161 (2008), Section 5.1.3, and reviewed references therein.
[2] Y. Utsuno, T. Otsuka, T. Mizusaki, and M. Honma, Phys. Rev. C **60**, 054315 (1999).
[3] A. Poves, E. Caurier, F. Nowacki, and K. Sieja, Phys. Scr. **2012**, 014030 (2012).
[4] E. Caurier, F. Nowacki, and A. Poves, Phys. Rev. C **90**, 014302 (2014).
[5] N. Tsunoda, T. Otsuka, N. Shimizu, M. Hjorth-Jensen, K. Takayanagi, and T. Suzuki, Phys. Rev. C **95**, 021304(R) (2017).
[6] A. Gade, P. Adrich, D. Bazin, M. D. Bowen, B. A. Brown, C. M. Campbell, J. M. Cook, T. Glasmacher, P. G. Hansen, K. Hosier, S. McDaniel, D. McGlinchery, A. Obertelli, K. Siwek, L. A. Riley, J. A. Tostevin, and D. Weisshaar, Phys. Rev. C **77**, 044306 (2008).
[7] B. A. Brown, P. G. Hansen, B. M. Sherrill, and J. A. Tostevin, Phys. Rev. C **65**, 061601(R) (2002).
[8] J. A. Tostevin and A. Gade, Phys. Rev. C **90**, 057602 (2014).
[9] J. A. Tostevin, Nucl. Phys. A **682**, 320 (2001).
[10] P. G. Hansen and J. A. Tostevin, Annu. Rev. Nucl. Part. Sci. **53**, 219 (2003).
[11] R. C. Johnson, in *Proc. Eur. Conf. On Advances in Nuclear Physics and Related Areas, Thessaloniki, Greece, July 8–12, 1997*, edited by D. M. Brink, M. E. Grypeos, and S. E. Massen (Giahoudi-Giapouli, Thessaloniki, 1999), p. 297.
[12] N. C. Summers, J. S. Al-Khalili, and R. C. Johnson, Phys. Rev. C **66**, 014614 (2002).
[13] F. Flavigny, A. Obertelli, A. Bonaccorso, G. F. Grinyer, C. Louchart, L. Nalpas, and A. Signoracci, Phys. Rev. Lett **108**, 252501 (2012).
[14] D. Bazin, R. J. Charity, R. T. de Souza, M. A. Famiano, A. Gade, V. Henzl, D. Henzlova, S. Hudan, H. C. Lee, S. Lukyanov, W. G. Lynch, S. McDaniel, M. Mocko, A. Obertelli, A. M. Rogers, L. G. Sobotka, J. R. Terry, J. A. Tostevin, M. B. Tsang, and M. S. Wallace, Phys. Rev. Lett. **102**, 232501 (2009).
[15] K. Wimmer, D. Bazin, A. Gade, J. A. Tostevin, T. Baugher, Z. Chajecki, D. Coupland, M. A. Famiano, T. K. Ghosh, G. F. Grinyer, M. E. Howard, M. Kilburn, W. G. Lynch, B. Manning, K. Meierbachtol, P. Quarterman, A. Ratkiewicz, A. Sanetullaev, S. R. Stroberg *et al.*, Phys. Rev. C **90**, 064615 (2014).
[16] A. E. L. Dieperink and T. L. de Forest, Jr., Phys. Rev. C **10**, 543 (1974).

[17] J. R. Terry, D. Bazin, B. A. Brown, J. Enders, T. Glasmacher, P. G. Hansen, B. M. Sherrill, and J. A. Tostevin, Phys. Rev. C **69**, 054306 (2004).

[18] A. Gade, D. Bazin, B. A. Brown, C. M. Campbell, J. A. Church, D. C. Dinca, J. Enders, T. Glasmacher, P. G. Hansen, Z. Hu, K. W. Kemper, W. F. Mueller, H. Olliver, B. C. Perry, L. A. Riley, B. T. Roeder, B. M. Sherrill, J. R. Terry, J. A. Tostevin, and K. L. Yurkewicz, Phys. Rev. Lett. **93**, 042501 (2004).

[19] B. A. Brown, Phys. Rev. C **58**, 220 (1998).

[20] D. A. Divaratne, C. R. Brune, H. N. Attanayake, T. Baumann, D. Bazin, A. Gade, S. M. Grimes, P. M. King, M. Thoennessen, and J. A. Tostevin, Phys. Rev. C **98**, 024306 (2018).

[21] S. Momiyama, K. Wimmer, D. Bazin, J. Belarge, P. Bender, B. Elman, A. Gade, K. W. Kemper, N. Kitamura, B. Longfellow, E. Lunderberg, M. Niikura, S. Ota, P. Schrock, J. A. Tostevin, and D. Weisshaar, Phys. Rev. C **102**, 034325 (2020).

[22] S. Jongile, A. Lemasson, O. Sorlin, M. Wiedeking, P. Papka, D. Bazin, C. Borcea, R. Borcea, A. Gade, H. Iwasaki, E. Khan, A. Lepailleur, A. Mutschler, F. Nowacki, F. Recchia, T. Roger, F. Rotaru, M. Stanoiu, S. R. Stroberg, J. A. Tostevin *et al.*, Phys. Rev. C **102**, 024321 (2020).

[23] A. Mutschler, O. Sorlin, A. Lemasson, D. Bazin, C. Borcea, R. Borcea, A. Gade, H. Iwasaki, E. Khan, A. Lepailleur, F. Recchia, T. Roger, F. Rotaru, M. Stanoiu, S. R. Stroberg, J. A. Tostevin, M. Vandebrouck, D. Weisshaar, and K. Wimmer, Phys. Rev. C **93**, 034333 (2016).

[24] A. Gade, R. V. F. Janssens, J. A. Tostevin, D. Bazin, J. Belarge, P. C. Bender, S. Bottoni, M. P. Carpenter, B. Elman, S. J. Freeman, T. Lauritsen, S. M. Lenzi, B. Longfellow, E. Lunderberg, A. Poves, L. A. Riley, D. K. Sharp, D. Weisshaar, and S. Zhu, Phys. Rev. C **99**, 011301(R) (2019).

[25] A. Gade, B. A. Brown, J. A. Tostevin, D. Bazin, P. C. Bender, C. M. Campbell, H. L. Crawford, B. Elman, K. W. Kemper, B. R. Longfellow, E. Lunderberg, D. M. Rhodes, and D. Weisshaar, Phys. Rev. Lett. **122**, 222501 (2019).

[26] A. Gade and B. M. Sherrill, Phys. Scr. **91**, 053003 (2016).

[27] N. Kobayashi, T. Nakamura, Y. Kondo, J. A. Tostevin, N. Aoi, H. Baba, R. Barthelemy, M. A. Famiano, N. Fukuda, N. Inabe, M. Ishihara, R. Kanungo, S. Kim, T. Kubo, G. S. Lee, H. S. Lee, M. Matsushita, T. Motobayashi, T. Ohnishi, N. A. Orr *et al.*, Phys. Rev. C **93**, 014613 (2016).

[28] Y. Yoshitome, Masters thesis, Tokyo Institute of Technology, 2021; Y. Yoshitome, Y. Kondo, T. Nakamura, J. A. Tostevin, and R. Tanaka *et al.*, RIKEN Accelerator Progress Report, Vol. 54 (unpublished).

[29] Y. X. Zhao, Y. Z. Sun, S. T. Wang, Z. Y. Sun, X. H. Zhang, D. Yan, D. Y. Pang, P. Ma, Y. H. Yu, K. Yue, S. W. Tang, S. M. Wang, F. Fang, Y. Sun, Z. H. Cheng, X. M. Liu, H. R. Yang, C. G. Lu, and L. M. Duan, Phys. Rev. C **100**, 044609 (2019).

[30] H. N. Liu, J. Lee, P. Doornenbal, H. Scheit, S. Takeuchi, N. Aoi, K. A. Li, M. Matsushita, D. Steppenbeck, H. Wang, H. Baba, E. Ideguchi, N. Kobayashi, Y. Kondo, G. Lee, S. Michimasa, T. Motobayashi, A. Poves, H. Sakurai, M. Takechi *et al.*, Phys. Lett. B **767**, 58 (2017).

[31] I. Murray, M. MacCormick, D. Bazin, P. Doornenbal, N. Aoi, H. Baba, H. Crawford, P. Fallon, K. Li, J. Lee, M. Matsushita, T. Motobayashi, H. Sakurai, H. Scheit, D. Steppenbeck, S. Takeuchi, J. A. Tostevin, N. Tsunoda, Y. Utsuno, H. Wang *et al.*, Phys. Rev. C **99**, 011302(R) (2019).

[32] B. A. Brown and W. A. Richter, Phys. Rev. C **74**, 034315 (2006).

[33] T. L. Tang, T. Uesaka, S. Kawase, D. Beaumel, M. Dozono, T. Fujii, N. Fukuda, T. Fukunaga, A. Galindo-Uribarri, S. H. Hwang, N. Inabe, D. Kameda, T. Kawahara, W. Kim, K. Kisamori, M. Kobayashi, T. Kubo, Y. Kubota, K. Kusaka, C. S. Lee *et al.*, Phys. Rev. Lett. **124**, 212502 (2020).

[34] S. E. Schlemme, Ph.D. thesis. Technische Universität Darmstadt, 2019, available at: https://tuprints.ulb.tu-darmstadt.de/8843/.

[35] G. F. Grinyer, D. Bazin, A. Gade, J. A. Tostevin, P. Adrich, M. D. Bowen, B. A. Brown, C. M. Campbell, J. M. Cook, T. Glasmacher, S. McDaniel, A. Obertelli, K. Siwek, J. R. Terry, D. Weisshaar, and R. B. Wiringa, Phys. Rev. C **86**, 024315 (2012).

[36] T. Aumann, C. Barbieri, D. Bazin, C. A. Bertulani, A. Bonaccorso, W. H. Dickhoff, A. Gade, M. Gómez-Ramos, B. P. Kay, A. M. Moro, T. Nakamura, A. Obertelli, K. Ogata, S. Paschalis, and T. Uesaka, Prog. Part. Nucl. Phys. **118**, 103847 (2021).

[37] J. Lee, M. B. Tsang, D. Bazin, D. Coupland, V. Henzl, D. Henzlova, M. Kilburn, W. G. Lynch, A. M. Rogers, A. Sanetullaev, Z. Y. Sun, M. Youngs, R. J. Charity, L. G. Sobotka, M. Famiano, S. Hudan, D. Shapira, P. O'Malley, W. A. Peters, K. Y. Chae, and K. Schmitt, Phys. Rev. C **83**, 014606 (2011).

[38] F. Flavigny, A. Gillibert, L. Nalpas, A. Obertelli, N. Keeley, C. Barbieri, D. Beaumel, S. Boissinot, G. Burgunder, A. Cipollone, A. Corsi, J. Gibelin, S. Giron, J. Guillot, F. Hammache, V. Lapoux, A. Matta, E. C. Pollacco, R. Raabe, M. Rejmund *et al.*, Phys. Rev. Lett. **110**, 122503 (2013).

[39] B. P. Kay, J. P. Schiffer, and S. J. Freeman, Phys. Rev. Lett. **111**, 042502 (2013).

[40] L. Atar, S. Paschalis, C. Barbieri, C. A. Bertulani, P. Díaz Fernández, M. Holl, M. A. Najafi, V. Panin, H. Alvarez-Pol *et al.*, Phys. Rev. Lett. **120**, 052501 (2018).

[41] S. Kawase, T. Uesaka, T. L. Tang, D. Beaumel, M. Dozono, T. Fukunaga, T. Fujii, N. Fukuda, A. Galindo-Uribarri, S. Hwang, N. Inabe, T. Kawabata, T. Kawahara, W. Kim, K. Kisamori, M. Kobayashi, T. Kubo, Y. Kubota, K. Kusaka, C. Lee *et al.*, Prog. Theor. Exp. Phys. **2018**, 021D01 (2018).

[42] M. Gómez-Ramos and A. M. Moro, Phys. Lett. B **785**, 511 (2018).

[43] J. Díaz-Cortésa, J. Benlliure, J. L. Rodríguez-Sánchez, H. Álvarez-Pol, T. Aumann, C. A. Bertulani, B. Blank, E. Casarejose, D. Cortina-Gil, D. Dragosavaca, V. Föhr, A. Gargano, M. Gascón, W. Gawlikowicz, A. Heinz, K. Helariuttak, A. Kelić-Heil, S. Lukić, F. Montes, D. Pérez-Loureiro, L. Pieńkowski, K.-H. Schmidt *et al.*, Phys. Lett. B **811**, 135962 (2020).

[44] O. Hen, G. A. Miller, E. Piasetzky, and L. B. Weinstein, Rev. Mod. Phys. **89**, 045002 (2017).

[45] M. Duer *et al.*, Nature (London) **560**, 517 (2018).

[46] M. Duer *et al.*, Phys. Rev. Lett. **122**, 172502 (2019).

[47] O. Hen, M. Sargsian, L. B. Weinstein, E. Piasetzky, H. Hakobyan, D. W. Higinbotham *et al.*, Science **346**, 614 (2014).

[48] S. Paschalis, M. Petri, A. O. Macchiavelli, O. Hen, and E. Piasetzky, Phys. Lett. B **800**, 135110 (2020).